Effect of progress variable definition on the mass burning rate of premixed laminar flames predicted by the Flamelet Generated Manifold method

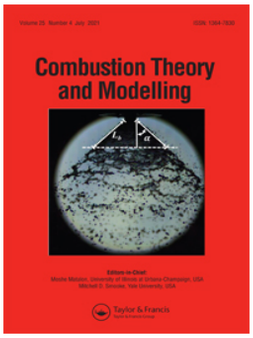

Taylor & Francis
Taylor & Francis Group

Combustion Theory and Modelling

ISSN: (Print) (Online) Journal homepage: https://www.tandfonline.com/loi/tctm20

Effect of progress variable definition on the mass burning rate of premixed laminar flames predicted by the Flamelet Generated Manifold method

Harshit Gupta, Omkejan J. Teerling & Jeroen A. van Oijen

To cite this article: Harshit Gupta, Omkejan J. Teerling & Jeroen A. van Oijen (2021) Effect of progress variable definition on the mass burning rate of premixed laminar flames predicted by the Flamelet Generated Manifold method, Combustion Theory and Modelling, 25:4, 631-645, DOI: 10.1080/13647830.2021.1926544

To link to this article: https://doi.org/10.1080/13647830.2021.1926544

Published online: 16 May 2021.

Combustion Theory and Modelling, 2021
Vol. 25, No. 4, 631–645, https://doi.org/10.1080/13647830.2021.1926544

Effect of progress variable definition on the mass burning rate of premixed laminar flames predicted by the Flamelet Generated Manifold method

Harshit Gupta [a,b*], Omkejan J. Teerling[a] and Jeroen A. van Oijen [b]

[a]*Bekaert Combustion Technology, Assen, Netherlands* [b]*Mechanical Engineering, Eindhoven University of Technology, Eindhoven, Netherlands*

(*Received 9 November 2020; accepted 26 April 2021*)

This paper investigates how the choice of progress variable in tabulated chemistry affects the mass burning rates of premixed laminar flames. Simulations are carried out using *finite rate, detailed chemistry (DC)* and *Flamelet Generated Manifolds (FGM)*. Through comparison of detailed chemistry and FGM (using different progress variable definitions), it is found that for FGM the mass burning rate depends on the choice of progress variable and thus results in a different mass burning rate than detailed chemistry. Since the mass burning rate is influenced by stretch and transport phenomena, the effects of these on mass burning rates are analysed. While FGM qualitatively predicts the effect of stretch on the mass burning rate compared to detailed chemistry, there are quantitative differences. It is shown that this is mainly caused by a lack of projection in usual FGM applications. When the projection of the source term and the diffusion term are included in the table, FGM becomes independent of the choice of progress variable and the effects of stretch are better represented by FGM similar to detailed chemistry.

Keywords: Flamelet Generated Manifolds; projection; flame speed; laminar flames; stretch

1. Introduction

Numerical modelling of combustion can be a useful tool to understand the underlying processes and how to manipulate them. Numerical modelling of combustion systems, however, is very challenging from a scientific point of view, especially for complex industrial systems where the interaction of the fluid flow, turbulence, chemical reactions and thermodynamics in reacting flows is of exceptional complexity [1,2]. Thus, usually and also in this study, the modelling of important physical aspects of combustion is limited to small reduced combustion problems with simplified versions of the real complex geometry of the appliance. To simplify combustion modelling an important assumption is exploited by researchers, namely, the fact that the chemical time and length scales in most flames are very small. This is used to reduce the number of equations to be solved leading to an enormous reduction in computation effort compared to detailed chemistry simulations.

Reduction techniques have been previously introduced and investigated by Mauss and Peters [3] and by Maas and Pope [4] who proposed the Intrinsic Low Dimensional Manifolds (ILDM) and also by Lam and Goussis [5] who proposed the Computational Singular

*Corresponding author. Email: harshit.gupta@bekaert.com

Perturbation (CSP) method. Bykov and Maas [6] further expanded the ILDM model to Reaction Diffusion Manifolds (REDIM) to better include transport phenomena. The Flamelet Generated Manifold (FGM) method as proposed by van Oijen and de Goey [7] is used in this study. The FGM method is similar to the Flamelet Prolongation of ILDM (FPI) method proposed by Gicquel et al. [8] and the Flamelet/Progress Variable (FPV) method proposed by Pierce and Moin [9]. While the analysis discussed in this paper is based on the FGM method, it can be applied to other manifold methods as well.

An FGM constitutes a composition space with a reduced dimension. The coordinates of this manifold are thermochemical variables which are called the control variables. For premixed flames, the progress variable is the primary control variable, which is usually a linear combination of species mass fractions used to define chemical reaction progress [7]. Non-reactive thermochemical variables like enthalpy, element mass fractions and pressure, have also been used as additional control variables to construct manifolds that can accommodate variations in these properties due to, e.g. mixing, heat loss, and preferential diffusion effects [7,10,11]. In this paper, we deliberately avoid these variations such that we can focus on the impact of the progress variable definition. In literature, many different definitions of progress variable can be found. Often linear combinations of mass fractions of major combustion products are used that are monotonously increasing when the reaction proceeds and result in a non-singular mapping of the composition as a function of the progress variable. Often such a suitable definition of the progress variable is found by trial and error, but various automatic optimisation techniques for the definition of the progress variable have been proposed by Niu et al. [12], Chen et al. [13], Ihme et al. [14] and others. These techniques rely mainly on improving the monotonicity of the progress variable and gradient reduction in the manifold. Therefore, these techniques can help reduce numerical errors such as data retrieval, interpolation and discretisation errors. The definition of progress variable does not only have an impact on numerical errors, but it also affects the physical modelling. Even if the numerical errors are minimised, different progress variables can still lead to different simulation results.

The basic assumption of manifold methods is that the evolution of the chemical system corresponds to a movement of the state on the manifold. The original full set of equations, however, contains terms that may drive the state off the manifold. In principle, these terms can be minimised by increasing the dimension of the manifold, but in practice it is not trivial to do this, mainly because it is not known in advance in which direction the manifold should be extended and how to span this space with flamelets. Another complementary method to guarantee that the chemical state remains on the manifold is to project the terms back on to the manifold. In this study, we investigate how the choice of progress variable affects the size and projection of these perturbation terms and hence the prediction of important flame properties, particularly the burning velocity of stretched flames. While projection and its necessity have been discussed previously by, e.g. Eggels [15], Strassacker et al. [16] and van Oijen et al. [17], it is the first time that projection is used in combination with FGM. The main novelty of this study, however, is the insight given in the impact of projection and the definition of progress variable on the prediction of the mass burning rate of stretched flames with the FGM method.

In this study, 1D adiabatic flame simulations are carried out using Chem1d [18] to produce FGM tables. These tables are utilised for calculating stretched adiabatic premixed laminar CH_4-air flames and the mass burning rates of these flames are compared with results calculated using detailed chemistry. The methodology behind the simulations is discussed in Section 2. In Section 3, it is shown that though qualitative agreements exist

between different progress variable choices and detailed chemistry, there are quantitative differences. These quantitative differences are further analysed by looking at the effects of projection of the chemical source and diffusion terms. It is shown that by projecting these terms the FGM simulation results can be made independent of the choice of progress variable irrespective of the equivalence ratio or the inlet temperature. Additionally, a method is proposed to predict the effect of the choice of progress variable on the mass burning rate without having to include projection in the FGM flame calculations. The conclusions and how this study can be used and applied in choosing the correct progress variable for future studies are discussed in the final section.

2. Methodology

In this section, we will briefly discuss the methodology behind the 1D simulations of premixed laminar flames. We will also show how the choice of progress variable can affect the outcome of an FGM calculation.

2.1. *One-dimensional stretched flames*

Simulations are carried out for 1D premixed laminar adiabatic flat flames using the Chem1d code [18]. Chem1d solves the following set of 1D conservation equations for mass, species mass fraction and energy:

$$\frac{\partial \rho u}{\partial x} + \rho K = 0, \tag{1a}$$

$$\frac{\partial \rho u Y_i}{\partial x} + \rho K Y_i = \frac{\partial}{\partial x}\left(\rho D_i \frac{\partial Y_i}{\partial x}\right) + \omega_i, \quad i = 1, \ldots, n_\mathrm{s} - 1, \tag{1b}$$

$$\frac{\partial \rho u h}{\partial x} + \rho K h = \frac{\partial}{\partial x}\left(\frac{\lambda}{c_p}\frac{\partial h}{\partial x}\right), \tag{1c}$$

where x is the spatial coordinate, t is time, ρ is density and u is the velocity. The strain rate is denoted by K, which for the steady flat flames considered in this paper is equal to the stretch rate. In mass conservation equation (1a), the first left-hand term represents the convective mass flux in the x-direction and the second left-hand term describes the mass loss/gain due to stretch, which corresponds to changes in the mass by fluxes in the other directions. Similar terms are present in the species mass fraction Y_i and enthalpy h balance equations. To impose $\sum Y_i = 1$, the mass fraction of the last species (N_2) is computed as $Y_{n_\mathrm{s}} = 1 - \sum_1^{n_\mathrm{s}-1} Y_i$. The first right-hand term in these two equations refers to the change caused by diffusive fluxes with D_i the mass diffusion coefficient, λ the thermal conductivity and c_p the specific heat capacity at constant pressure. The last term in species equation (1b) represents the source term ω_i due to chemical reactions.

It is well known that flame stretch has a direct effect on the mass burning rate of premixed flames [10,19]. However, it also has an indirect effect due to preferential diffusion which causes changes in enthalpy and element mass fractions leading to changes in flame temperature and reaction rates. Although these effects can be included in the FGM method using additional manifold dimensions [10,20], they are neglected here in order to isolate the effect of the choice of progress variable and to prevent the analysis from becoming unnecessarily complex. To remove the preferential diffusion effects, a unity Lewis number ($\mathrm{Le}_i = 1$) assumption is used for all species, which implies that all diffusion coefficients in equation set (1) are equal, viz. $\rho D_i = \lambda / c_p = \rho D$.

For specific configurations, such as a stagnation flow, an equation for the stretch rate K can be derived from the momentum equation. However, in the present study, a constant stretch rate field K is prescribed in the flame zone following previous studies [10,21]. Similar to unstretched 1D freely propagating flames, the set of equations is solved by treating it as an eigenvalue problem with the mass burning rate ρu at the location of the flame as an eigenvalue of the system.

2.2. *Flamelet-Generated Manifolds*

In manifold methods, such as FGM, the thermochemical composition is described by a reduced set of variables. The full set of variables that describes the thermochemical composition in a flame consists of $n_\mathrm{s} - 1$ independent species mass fractions and enthalpy, which can be represented by the vector $\boldsymbol{y} = (Y_1, Y_2, \ldots, Y_{n_\mathrm{s}-1}, h)$. The elements of this vector correspond to the coordinates of an n_s-dimensional composition space. In manifold methods, it is assumed that the composition is restricted to a lower-dimensional manifold in composition space. The complete composition can then be described by a reduced number of variables, which are the coordinates of the manifold. These coordinates are often referred to as the control variables, and they can be represented by a vector $\boldsymbol{\eta} = (\eta_1, \eta_2, \ldots, \eta_{n_\mathrm{r}})$ with n_r the dimension of the manifold.

In the FGM method, the manifold is found by solving a set of flamelet equations. Its solution is a one-dimensional flame, which corresponds to a 1D curve in composition space. The single coordinate and control variable of this 1D manifold is referred to as the progress variable. Often additional manifold dimensions are needed, for instance, to account for changes in enthalpy and element mass fractions [10]. In the present case, however, these extra dimensions are not required. The investigated flames are adiabatic and due to the unity Lewis number assumption, preferential diffusion effects are absent, which implies that the enthalpy and element mass fractions are constant. In [11], it was shown that in such a case a 1D manifold is sufficient for accurate predictions of premixed counterflow flames up to the point of extinction.

The governing equations for the control variables are derived from the governing equations for the full set of variables $\boldsymbol{y} = (Y_1, Y_2, \ldots, Y_{n_\mathrm{s}-1})$, where we have dropped h because it is constant. Using this vector notation, the unsteady, three-dimensional equations can be written as

$$\rho \frac{\partial \boldsymbol{y}}{\partial t} + \rho \boldsymbol{u} \cdot \nabla \boldsymbol{y} = \nabla \cdot (\rho D \nabla \boldsymbol{y}) + \boldsymbol{\omega}, \tag{2}$$

where $\boldsymbol{\omega} = (\omega_1, \omega_2, \ldots, \omega_{n_\mathrm{s}-1})$. The control variables are typically linear combinations of the original variables $\boldsymbol{\eta} = \mathbf{A}\boldsymbol{y}$ with $\mathbf{A}$ a constant $n_\mathrm{r} \times (n_\mathrm{s} - 1)$ matrix defining the control variables. The row vectors of $\mathbf{A}$ consist of the weights of the species mass fractions in the definition of the control variables. The transport equations for the control variables are usually derived by taking the corresponding linear combinations of the original species equations. Multiplying vector equation (2) by $\mathbf{A}$ yields an equation for $\boldsymbol{\eta}$:

$$\rho \frac{\partial \boldsymbol{\eta}}{\partial t} + \rho \boldsymbol{u} \cdot \nabla \boldsymbol{\eta} = \nabla \cdot (\rho D \nabla \boldsymbol{\eta}) + \boldsymbol{\omega}_{\boldsymbol{\eta}}, \tag{3}$$

where $\boldsymbol{\omega}_{\boldsymbol{\eta}} = \mathbf{A}\boldsymbol{\omega}$. These equations are of the same convection–diffusion–reaction type as the original species equations (2) and are, therefore, relatively easy to implement in existing flow solvers, which has certainly contributed to the widespread use of the method.

In order to explain the effect of the definition of the control variables on the model, we first introduce a simplified notation of (2):

$$\frac{\mathrm{D}\boldsymbol{y}}{\mathrm{D}t} = \boldsymbol{w}, \tag{4}$$

where $\frac{\mathrm{D}}{\mathrm{D}t} = \frac{\partial}{\partial t} + \boldsymbol{u} \cdot \nabla$ is the material derivative and $\boldsymbol{w}$ the right-hand side of (2) divided by ρ. Note that $\boldsymbol{w}$ consists of the chemical source term and the diffusion term and should not be confused with $\boldsymbol{\omega}$. Equation (4) expresses that the composition of a gas parcel moving with the flow velocity changes due to diffusion and chemical reactions. The vector $\boldsymbol{w}$ corresponds to the change of the state in composition space. Figure 1 shows this movement in composition space for a theoretical example, in which the composition lies on a 1D manifold M. Note that in general the vector $\boldsymbol{w}$ doesn't lie in the tangent space of the manifold due to phenomena that are not included in the flamelet equations when they are solved to generate the manifold.

In the example of Figure 1, both y_1 and y_2 are suitable choices as progress variable coordinate of the 1D manifold. If y_1 is used as a progress variable, the reduced system is governed by

$$\frac{\mathrm{D}y_1}{\mathrm{D}t} = w_1, \tag{5a}$$

$$y_i = f_i(y_1) \quad i \neq 1, \tag{5b}$$

which implies that y_1 follows from its transport equation, while the other species mass fractions are retrieved from the manifold using y_1 as coordinate. This is schematically shown by the solid w_1 lines in Figure 1(a). The solid w_1 arrow represents the change of y_1 by w_1, and the dashed w_1 line represents the lookup of y_2 in the manifold as a function of y_1. When y_2 is used as a progress variable, the reduced system is described by

$$\frac{\mathrm{D}y_2}{\mathrm{D}t} = w_2, \tag{6a}$$

$$y_i = f_i(y_2) \quad i \neq 2, \tag{6b}$$

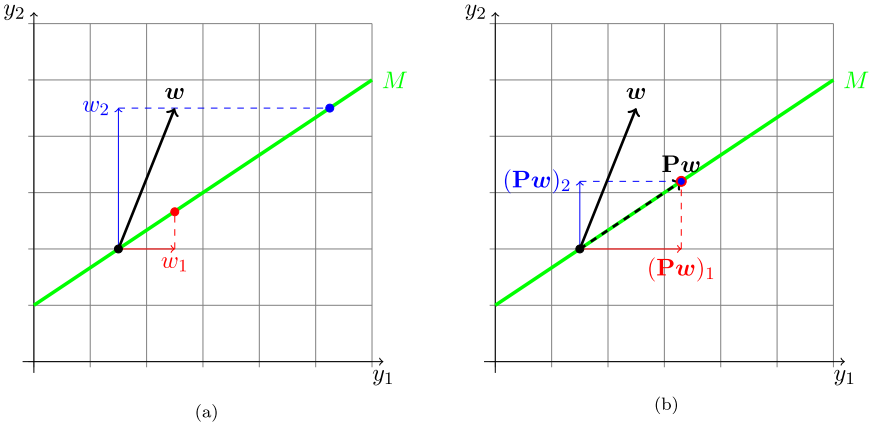

Figure 1. Movement of the thermochemical state along a one-dimensional manifold M in composition space for two different progress variables y_1 and y_2. (a) Without projection and (b) with projection.

which is represented by the w_2 lines in Figure 1(a). It is obvious that the two choices of progress variable result in a different movement along the manifold. When y_2 is used, a significantly larger change in composition is found.

The reason for this difference is the fact that $\boldsymbol{w}$ has a component normal to the tangent space of the manifold. In Figure 1(a), the projection back to the manifold is implicit, and thus, we refer to this approach as without projection. It corresponds to a projection perpendicular to the direction of the progress variable, which implies that the projected system depends on the choice of progress variable. To properly resolve this dependency, the vector $\boldsymbol{w}$ should first be projected onto the manifold. In that case, the reduced system is described by

$$\frac{\mathrm{D}\boldsymbol{y}}{\mathrm{D}t} = \mathbf{P}\boldsymbol{w}, \tag{7}$$

where $\mathbf{P}$ is a $(n_\mathrm{s}-1)\times(n_\mathrm{s}-1)$ matrix that projects the composition space on the tangent space of the manifold. Following Eggels and De Goey [22] and Strassacker et al. [16], we use an orthogonal projection matrix $\mathbf{P} = \mathbf{X}(\mathbf{X}^\mathrm{T}\mathbf{X})^{-1}\mathbf{X}^\mathrm{T}$, in which $\mathbf{X}$ is a $(n_\mathrm{s}-1)\times n_\mathrm{r}$ matrix with column vectors $\boldsymbol{x}_j$ that span the manifold, having elements $x_{ij} = \partial y_i/\partial\eta_j$.

Since $\mathbf{P}\boldsymbol{w}$ lies in the manifold, both progress variables lead to the same movement along the manifold, as shown by the dashed $\mathbf{P}\boldsymbol{w_1}$ and $\mathbf{P}\boldsymbol{w_2}$ lines in Figure 1(b).

Expanding $\boldsymbol{w}$ in its diffusion and reaction source terms, Equation (7) can be written as

$$\rho\frac{\mathrm{D}y_i}{\mathrm{D}t} = \nabla\cdot\left(\rho D P_{ij}\nabla y_j\right) - \rho D\nabla P_{ij}\cdot\nabla y_j + P_{ij}\omega_j, \quad i = 1,\ldots,n_\mathrm{s}-1, \tag{8}$$

where implicit summation over repeated indices is used. The second term on the right-hand side appears because the projection matrix $\mathbf{P}$ is placed after the gradient operator of the first term. Since $\mathbf{P}$ is not constant this leads to the second term with its gradient. Equation (8) describes the movement of the full system along the manifold. The equations for the reduced system are obtained by multiplying (8) by $\mathbf{A}$, which gives

$$\rho\frac{\mathrm{D}\eta_k}{\mathrm{D}t} = \nabla\cdot(\rho D\nabla\eta_k) - \rho D\frac{\partial Q_{kj}}{\partial\eta_l}\frac{\partial y_j}{\partial\eta_m}\nabla\eta_l\cdot\nabla\eta_m + Q_{kj}\omega_j, \quad k = 1,\ldots,n_\mathrm{r} \tag{9}$$

where $Q_{kj} = A_{ki}P_{ij}$ the elements of the $n_\mathrm{r}\times(n_\mathrm{s}-1)$ matrix $\mathbf{Q} = \mathbf{AP}$. Equation 9 is similar to the commonly used Equation (3) except for the last two terms on the right-hand side. The last term is the kth component of the projected chemical source term $\boldsymbol{\omega}_P = \mathbf{AP}\boldsymbol{\omega}$, while in (3) the source term is $\mathbf{A}\boldsymbol{\omega}$. The second term is related to the variation of the projection matrix along the manifold. To evaluate this term, an $n_\mathrm{r}\times n_\mathrm{r}$ matrix $\mathbf{B}_k$ with elements $B_{klm} = (\partial Q_{kj}/\partial\eta_l)/(\partial y_j/\partial\eta_m)$ needs to be stored in the lookup table for each control variable η_k.

In this paper, 1D manifolds are used ($n_\mathrm{r} = 1$). Therefore, the matrix $\mathbf{B}_k$ reduces to a scalar and the index k denoting the different control variables will be omitted from hereon. For the steady, one-dimensional, stretched flames discussed in the previous section, the set of FGM reduced equations including projection then becomes

$$\frac{\partial\rho u}{\partial x} + \rho K = 0, \tag{10a}$$

$$\frac{\partial\rho u\eta}{\partial x} + \rho K\eta = \frac{\partial}{\partial x}\left(\rho D\frac{\partial\eta}{\partial x}\right) - \rho DB\left(\frac{\partial\eta}{\partial x}\right)^2 + \omega_P. \tag{10b}$$

The convection term lies in the manifold by definition and is, therefore, not affected by a projection. This has been derived and explained previously by researchers such as Bykov and Maas [6] and Strassacker et al. [16]. The second diffusion term on the right-hand side of (10b) is implemented in the code by using second-order finite differences for the spatial derivative of η. The derivatives $\partial y_i/\partial \eta_j$ along the manifold, which are needed to construct **B** and **P**, are approximated with second-order finite differences.

The dimension of the manifold can be increased to improve the accuracy of the reduced model. By increasing the dimension of the manifold, the component of the vector pointing out of it is reduced, as well as the associated modelling error. Extending the manifold to higher dimensions is, however, not always straightforward. While it is common to add dimensions to account for variations in chemically conserved quantities such as enthalpy and element mass fractions [10,17,23], this is certainly not the case for extra dimensions to include additional reaction time scales. Additional dimensions to account for changes in the conserved variables as discussed in detail by van Oijen et al. [10] are not needed in the present work, because these quantities do not vary in the flames that are studied here. In general, adding more dimensions will enhance the accuracy, but one cannot guarantee that the state remains inside the manifold. Therefore, the projection should not be regarded as a replacement for adding more dimensions. The projection makes FGM more consistent and makes the results independent of the choice of progress variable.

2.3. *Simulation settings*

For all the simulations in this study, the fuel consists of pure CH_4 and the oxidiser consists of 21 mol% O_2 and 79 mol% N_2. The DRM19 reaction mechanism [24] is used in this study to calculate the chemical source terms. It is a reduced mechanism that was found to give very similar results for the present flames as more comprehensive mechanisms, such as GRI-mech 3.0 [25]. The simulations are carried out on a domain ranging from -2 to 10 cm discretised using 300 mesh points, whose location is adapted to the solution with clustering of points in the region of high gradients. This adaptive mesh refinement ensures that grid independence has been achieved at 300 grid points. The pressure is atmospheric. The main inlet conditions that are varied are (i) the equivalence ratio ϕ, ranging from lean to stoichiometric mixtures ($\phi = 0.8$, 0.9 and 1.0), and (ii) the inlet temperature $T_\mu = 300$, 500 and 700 K (for $\phi = 0.8$). A spatially uniform stretch rate ranging from $K = -200$ to 1000 s^{-1} is applied to study the effects of stretch on the mass burning rate. The results are presented in the following section.

3. Results and discussions

3.1. *Flame structure*

To investigate the role of the progress variable definition, 1D FGM simulations with different progress variables are compared with detailed chemistry results. Figure 2 shows the chemical source term ω_c as a function of the normalised progress variable c for two different progress variables, O_2 and CO_2. The normalisation is carried out as

$$c = \frac{\eta - \eta_\mathrm{u}}{\eta_\mathrm{b} - \eta_\mathrm{u}} \quad \text{and} \quad \omega_c = \frac{\omega_\eta}{\eta_\mathrm{b} - \eta_\mathrm{u}}, \tag{11}$$

where the subscripts u and b refer to the values of the unburnt and burnt mixture, respectively. It can be seen that the peak source term for O_2 is almost twice higher and occurs

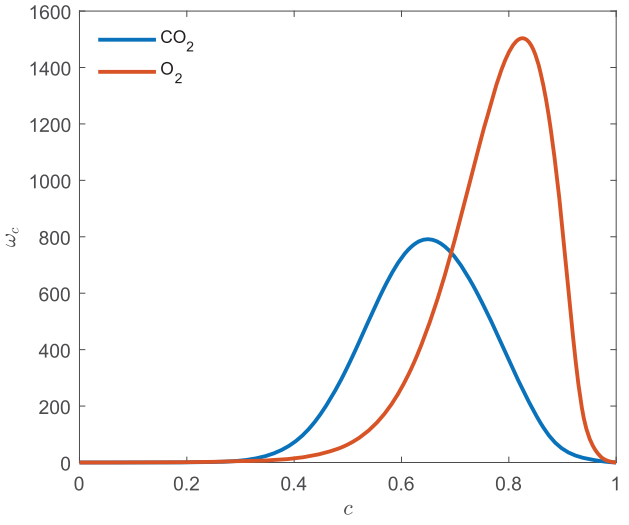

Figure 2. Chemical source terms ω_c of normalised progress variables c based on O_2 and CO_2 for $\phi = 0.8$ and $T_\mu = 300\,K$.

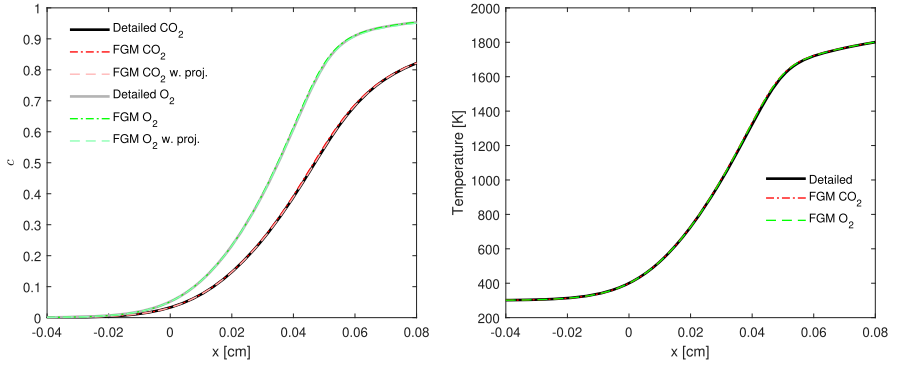

Figure 3. Normalised progress variable and temperature profiles of an unstretched flame ($K = 0\,s^{-1}$) for detailed and FGM chemistry simulations. (a) Normalised progress variable c and (b) temperature.

at higher values of the normalised progress variable than the profile for CO_2 as a progress variable. This difference in source term profiles indicates that using either species as a progress variable will probably result in different flame behaviour.

The spatial profiles of both progress variables and temperature are shown in Figure 3 for an unstretched flame. The profiles of detailed chemistry simulations are compared with results of FGM calculations with and without projection. It is obvious that the two progress variables result in different profiles for c. The larger source term for O_2 leads to a steeper c profile. The results of the FGM calculations are in excellent agreement with the detailed simulations. Apart from very small numerical errors, the FGM profiles are identical to the detailed ones, because the flame that is simulated is also used to construct the manifold. This also implies that there are no processes driving the state of the manifold, which need

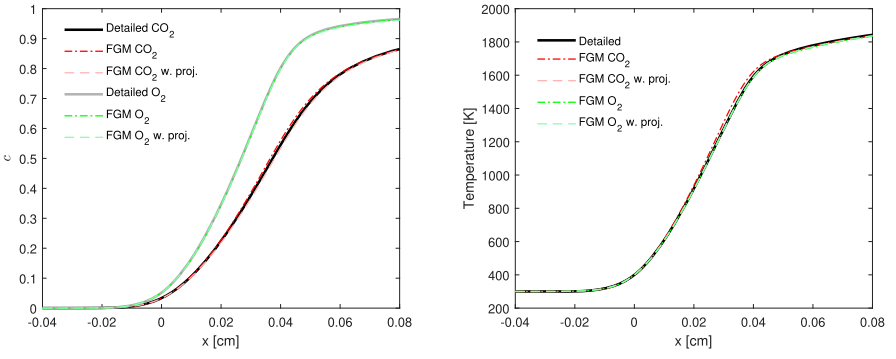

Figure 4. Normalised progress variable, temperature and mass flux profiles of a stretched flame ($K = 1000\,\mathrm{s}^{-1}$) for detailed and FGM chemistry simulations. (a) Normalised progress variable c and (b) temperature and mass flux.

to be projected. As a consequence, the FGM simulation results with projection are identical to the ones without. Figure 3(b) shows that although the progress variable profiles are quite different, the temperature profiles are identical for the FGM simulations with different progress variables. The FGM simulations with projection give identical temperature profiles as the simulations without projection because their computed c profiles are identical. Therefore, the FGM results with projection are not included in the temperature plot.

Stretch ($K = 1000\,\mathrm{s}^{-1}$) is subsequently applied to the flames shown in Figure 3, and the spatial profiles of both progress variable and temperature are shown in Figure 4. The progress variable profiles in Figure 4(a) show that the stretched flames are slightly compressed compared to unstretched flames in Figure 3(a). This compression, however, does not seem to affect the behaviour of the progress variable also shown previously by van Oijen [26]. Stretch is not included while creating the flamelets, so this results in differences between FGM and detailed chemistry. Unlike unstretched flames, the profile of progress variable for FGM calculations is affected by the choice of progress variable and the inclusion of projection in the FGM table. Figure 4(a) shows that O_2 profiles for flames with and without projection are identical to detailed chemistry similar to unstretched flames. However, the CO_2 FGM results without projection deviate slightly from the detailed chemistry. Similar to unstretched flames the temperature profiles for FGM solutions with projection is independent of the choice of progress variable. For FGM flame simulations without projection, CO_2 as a progress variable deviates from detailed chemistry while O_2 does not. This shows that without projection the choice of progress variable affects the FGM flame simulations when they are stretched.

Following the mass balance equation (Equation (1a)), the mass flux ρu decreases as a function of the spatial coordinate when the flame is stretched positively. This change in mass flux for the stretched flames is shown in Figure 4(b). The change in mass flux for FGM flames with O_2 as a progress variable seems identical to detailed chemistry, with or without projection. However, for CO_2 FGM calculations without projection, the mass flux deviates from the detailed chemistry. This change in mass flux will affect the mass burning rate of stretched flames, which is studied in the following subsection.

3.2. *Mass burning rate and Markstein number*

The mass burning rate is defined as the product of density and burning velocity, $m = \rho s_L$. For steady flames, the burning velocity equals the gas velocity and, therefore, $m = \rho u$. The mass flux changes in the flame structure due to applied stretch following from Equation (1) as shown in Figure 4(b), hence the mass burning rate depends on the location at which it is evaluated. Following our previous work [10,11,19], we take the mass burning rate m_b at the burned side of the flame, i.e. at the location where the heat release rate has dropped to 10% of its maximum value.

Dimensionless mass burning rates (m_b/m_b^0) of flames computed with the aforementioned and other traditional progress variables (prevalently found in the literature [20,26]) are plotted in Figure 5 against Karlovitz number Ka. The Karlovitz number is a dimensionless stretch rate defined here as $\mathrm{Ka} = \rho_b^0 \delta_f^0 K/m_b^0$ with δ_f the flame thickness based on the maximum temperature gradient. Here the superscript 0 represents values of the unstretched flame. An optimised progress variable is also studied, for which the required species and their weight coefficients A_i are found using the optimisation process as discussed by Niu et al. [12] and Chen et al. [13] and are given in Table 1. The FGM calculations presented in Figure 5 are performed without projection.

While all the FGMs with different progress variables are able to qualitatively predict the effect of stretch on the mass burning rate as can be seen in Figure 5, there are quantitative differences between them. It is also clear that especially CO_2 as a progress variable deviates the most from the detailed chemistry results, but it is also qualitatively different from the other progress variable choices shown here. While CO_2 under-predicts the

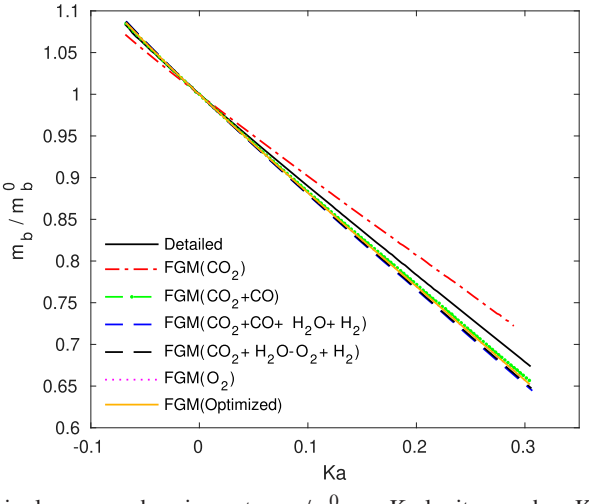

Figure 5. Dimensionless mass burning rate m_b/m_b^0 vs. Karlovitz number Ka computed using detailed chemistry and FGM with different progress variables and without projection.

Table 1. Species and their weight factors A_i defining the optimised progress variable.

Species	O	O_2	H_2O	CH_4	CO	CO_2
A_i	0.5515	− 5.5866	0.0073	− 0.0181	0.0272	0.0237

decrease in the mass burning rate for positive stretch compared to detailed chemistry, the other progress variables over predict the stretch effect. This difference is probably caused by the lack of projection as previously discussed. While the progress variable optimisation process reduces interpolation errors, it doesn't improve upon the prediction of stretch effects. The optimised progress variable gives comparable results to the other traditional progress variables with no clear advantage.

In Figure 5, CO_2 and O_2 seem to be the furthest from the detailed chemistry results in opposite directions, while other progress variables are relatively close to each other. To carry out a parametric study, a set of combined progress variable $\eta = aY_{CO_2} + (1-a)Y_{O_2}$ with $a = 0,\ 0.25,\ 0.75,\ 1$ is investigated, such that at $a = 1.0$ the progress variable is the mass fraction of CO_2 and at $a = 0$ it equals the mass fraction of O_2. Using these progress variables, FGM simulations of stretched flames are performed with and without projection. The resulting mass burning rates m_b are shown against Karlovitz number in Figure 6. Without projection there is a clear continuous transition between the CO_2 and O_2 progress variables as shown in Figure 6(a). The projected solutions in Figure 6(b), however, become independent of the choice of progress variable in agreement with theory. Note that a difference varying from $+4\%$ to $+14\%$ with the detailed chemistry results remains, depending on the boundary condition. This difference is caused by the modelling error that is introduced by the 1D FGM assumption. After all, the chemical source term $\omega_c(c)$ of a stretched flame is not exactly the same as that of a stretchless flame, which is used to generate the manifold.

In order to quantify the differences between the results of different progress variables and detailed chemistry, Markstein numbers, Ma, are calculated using the definition

$$\frac{m_b}{m_b^0} = 1 - \mathrm{Ma}\,\mathrm{Ka}. \tag{12}$$

A second-order polynomial is fitted to the numerical m_b/m_b^0 vs. Ka results and the Markstein number is computed as the derivative of this fit at $\mathrm{Ka} = 0$. The Markstein numbers for the FGM simulations are compared with detailed chemistry simulations for different inlet temperatures $T_\mu = 300$, 500 and 700 K, and equivalence ratios $\phi = 0.8$, 0.9 and 1.0 in Table 2.

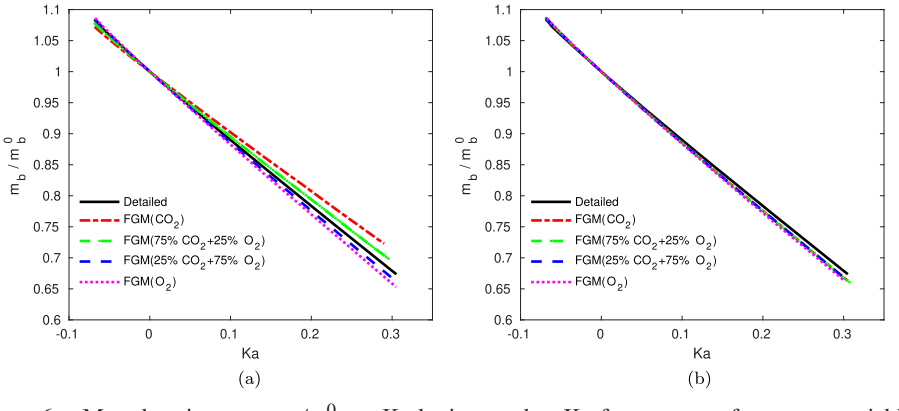

Figure 6. Mass burning rate m_b/m_b^0 vs. Karlovitz number Ka for a range of progress variables computed (a) without and (b) with projection.

Table 2. Markstein numbers for detailed chemistry and FGM simulations with and without projection at various unburnt temperatures T_μ and equivalence ratio ϕ.

			FGM without projection				FGM with projection			
T_μ [K]	ϕ	Detailed	$a = 1.0$	0.75	0.25	0.0	1.0	0.75	0.25	0.0
300	0.8	1.14	1.00	1.08	1.17	1.20	1.18	1.18	1.18	1.19
500	0.8	1.03	0.89	0.98	1.08	1.11	1.10	1.10	1.10	1.11
700	0.8	0.90	0.80	0.90	1.01	1.04	1.04	1.04	1.04	1.04
300	0.9	1.07	0.94	1.02	1.11	1.14	1.12	1.12	1.12	1.13
300	1.0	1.05	0.92	0.99	1.08	1.11	1.10	1.10	1.10	1.11

Markstein numbers of FGM flames with projection seem to be approximately the same when compared with those of FGM flames without projection as shown in Table 2. However, there is still a difference after projection when compared with detailed chemistry. The FGM method without projection leads to a larger relative difference (detailed chemistry vs. FGM) for Ma, approximately -10% for CO_2 ($a = 1$) and $+8\%$ for O_2 ($a = 0$) at $T_\mu = 300\,\mathrm{K}$ and $\phi = 0.8$. When projection is applied, all the progress variable results for these boundary conditions have the same relative difference of about $+3\%$ compared to the detailed chemistry. Therefore, with projection the Markstein number is independent of the progress variable (i.e. a) as was shown for this condition in Figure 6(b). The results for the other conditions confirm that, irrespective of the change in inlet temperature or equivalence ratio, the inclusion of projection in FGM simulations makes the mass burning rate prediction independent of the choice of progress variable.

It can also be seen that some progress variables (e.g. $a = 0.25$) lead to rather small differences in Ma without projection, which might be acceptable for applications of FGM. In the following subsection, we present a parameter that can help choose an optimum progress variable without having to use projection in more complex FGM calculations.

3.3. *Optimal progress variable for simulations without projection*

For the present one-dimensional manifold, the projection is rather straightforward to implement. For a multi-dimensional manifold, the projection becomes more complex and time-consuming due to the extra diffusion cross-terms in Equation (9). To avoid projection when doing calculations with multi-dimensional manifolds, we investigate whether the possible deviation of the FGM solution for a given progress variable can be used to calculate the projected diffusion term in Equation (10b) for an unstretched flame. The different terms in Equation (10b) for CO_2 and O_2 are displayed in Figure 7. As expected, the convection and diffusion terms balance in the preheat zone of the flame. In the reaction zone, all terms are significant, including the additional diffusion term due to projection. The profile of this diffusion term depends on the choice of the progress variable. The absolute maximum is higher and positive for CO_2 and vice versa for O_2.

Since the additional diffusion term in (10b) and the projection of the source term are the only differences with respect to the unprojected case, the magnitude of the additional term can be regarded as a measure of the importance of projection for a certain progress variable choice. The idea is that if this term is small for a certain progress variable, that the projection will not be important and that the results of simulations without projection are similar to results of simulation with projection. To quantify the magnitude of the additional

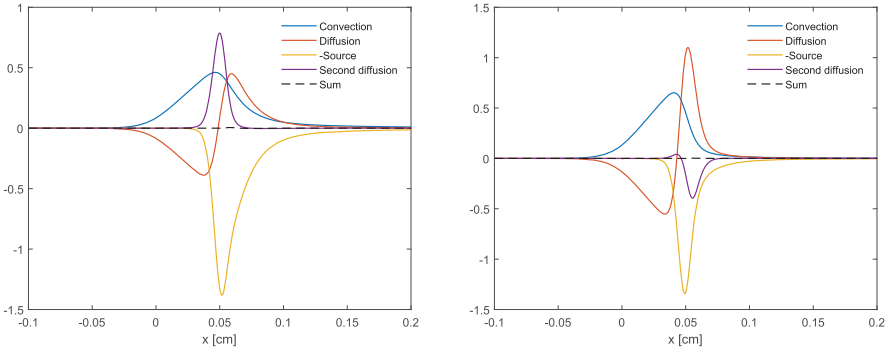

Figure 7. Different terms in the projected balance equation for the normalised mass fractions of (a) CO_2 and (b) O_2 for an unstretched flame.

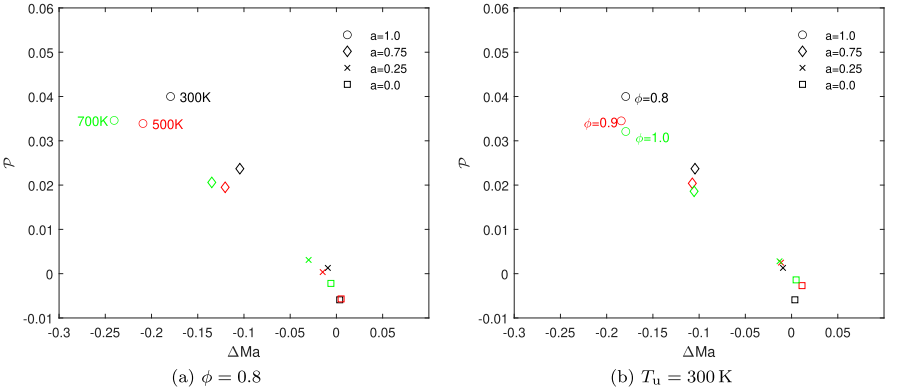

Figure 8. Integrated additional diffusion term $\mathcal{P}$ vs. the difference in Markstein numbers ΔMa of FGM simulations with and without projection. (a) $\phi = 0.8$ and (b) $T_\mu = 300\,K$.

diffusion term, the variable $\mathcal{P}$ is defined as the integral of the absolute term scaled by the integrated convection term:

$$\mathcal{P} = \frac{\int_{-\infty}^{\infty} \rho D B \left(\frac{\partial \eta}{\partial x}\right)^2 \mathrm{d}x}{\int_{-\infty}^{\infty} \frac{\partial}{\partial x}(\rho u \eta)\,\mathrm{d}x} = \frac{1}{m_\mathrm{b}^0} \int_{-\infty}^{\infty} \rho D B \left(\frac{\partial \eta}{\partial x}\right)^2 \mathrm{d}x, \tag{13}$$

where we have used that the integrated convective term is equal to m_b^0. This quantity $\mathcal{P}$ is plotted in Figure 8 for different progress variables and different inlet conditions. It is plotted against the difference in the Markstein numbers $\Delta\mathrm{Ma} = \mathrm{Ma}_\mathrm{wop} - \mathrm{Ma}_\mathrm{wp}$ between the FGM simulations without and with projection indicated by the subscripts wop and wp, respectively.

$\mathcal{P}$ and ΔMa have a strong correlation which can be used to predict the behaviour of FGM tables without projection. In Figure 8, CO_2 has the highest $\mathcal{P}$, while O_2 has the lowest $\mathcal{P}$; they also have the highest and lowest ΔMa, respectively. Similar to the previous results of the mass burning rate and the Markstein number, other choices of the progress variable fall between the two mono-species progress variables. This is similar to the mass burning rate change with stretch as seen in Figure 6, especially when compared with detailed chemistry.

Comparing $\mathcal{P}$ for different progress variables at different inlet boundary conditions, we can see that the choice of CO_2 as a species to define the progress variable will lead to quantitatively larger difference than other choices of progress variable especially O_2. This quantity can also help predict if the choice of progress variable will over predict ($\mathcal{P} > 0$ for CO_2) or under predict ($\mathcal{P} \leq 0$ for O_2) the change in the mass burning rate due to stretch with respect to detailed chemistry. When absolute values are taken of the integral quantity in Equation (13), it shows similar relation between $\mathcal{P}$ and ΔMa; it does not provide the additional information regarding under/over prediction of the mass burning rate with respect to detailed chemistry.

4. Conclusions and discussions

In this study, we focused on 1D flat adiabatic premixed flame where we compared stretched flames simulated using detailed chemistry and FGM (different progress variables). It was shown that while FGM reproduces the qualitative effects of stretch on the mass burning rate there exist a quantitative difference between FGM and detailed chemistry, especially between different progress variables. We showed that this dependence on the choice of progress variable originates due to the lack of inclusion of projection in the FGM tables. While previous authors have neglected these errors due to the scale of this error, the inclusion of projection can help remove this dependence. We studied the effect of projection by looking at the characteristic property of stretched flame, the Markstein number. Markstein numbers were used to quantify this difference, which showed that CO_2 as a progress variable gives an accuracy error of -10% while O_2 gives an error of approximately $+8\%$ when compared with detailed chemistry.

Projection in simplified 1D FGM flames is shown to be simple but this can quickly become numerically intensive with additional FGM dimensions or inclusion of turbulence etc. We proposed that by calculating the size of the projected perturbation $\mathcal{P}$ (secondary diffusion term in the projected progress variable transport equation) researchers can make early predictions on how the choice of their progress variable will affect the stretched mass burning rate in their future studies, without having to calculate stretched mass burning rates of different progress variables and detailed chemistry. It should be noted that monotonicity still governs the choice of progress variable. However, if there are multiple progress variable choices available, the optimal progress variable can be chosen using $\mathcal{P}$.

The projection as discussed in this paper can be straightforwardly applied to manifold based direct numerical simulation of turbulent flames. For unresolved simulations (RANS or LES), averaging should be applied to the projected equations, which will lead to unresolved terms that need to be closed. Though projection was shown to affect the simulation results, other modelling choices in such simulations of turbulent flames might have larger effects. The quantitative contribution of projection and progress variable choice in simulations of turbulent flames remains to be investigated.

Disclosure statement

No potential conflict of interest was reported by the author(s).

ORCID

Harshit Gupta http://orcid.org/0000-0003-4632-2622
Jeroen A. van Oijen http://orcid.org/0000-0002-4283-2898

References

[1] C.K. Law, *Combustion[Q7] Physics*, Cambridge University Press, Cambridge, 2006.

[2] J. Warnatz, U. Maas, and R.W. Dibble, *Combustion: Physical and Chemical Fundamentals, Modeling and Simulation, Experiments, Pollutant Formation*, Springer Berlin Heidelberg, Berlin, Heidelberg, 2006.

[3] F. Mauss and N. Peters, *Reduced Kinetic Mechanisms for Premixed Methane-Air Flames*, Springer Berlin Heidelberg, Berlin, Heidelberg, 1993.

[4] U. Maas and S.B. Pope, Simplifying chemical kinetics: Intrinsic low-dimensional manifolds in composition space, Combust. Flame 88 (1992), pp. 239–264.

[5] S.H. Lam and D.A. Goussis, *Understanding complex chemical kinetics with computational singular perturbation*. Proc. Combust. Inst. 22 (1988), pp. 931–941.

[6] V. Bykov and U. Maas, The extension of the ildm concept to reaction-diffusion manifolds, Combust. Theory Model. 11 (2007), pp. 839–862.

[7] J.A. van Oijen and de Goey L.P.H., Modelling of premixed laminar flames using flamelet-generated manifolds, Combust. Sci. Technol. 161 (2000), pp. 113–137.

[8] O. Gicquel, N. Darabiha, and D. Thévenin, Laminar premixed hydrogen/air counterflow flame simulations using flame prolongation of ildm with differential diffusion, Proc. Combust. Inst. 28 (2000), pp. 1901–1908.

[9] C.D. Pierce and P. Moin, Progress-variable approach for large-Eddy simulation of non-premixed turbulent combustion, J. Fluid. Mech. 504 (2004), pp. 73–97.

[10] J.A. van Oijen, A. Donini, R.J.M. Bastiaans, ten Thije Boonkkamp J.H.M., and de Goey L.P.H., State-of-the-art in premixed combustion modeling using flamelet generated manifolds, Prog. Energy Combust. Sci. 57 (2016), pp. 30–74.

[11] J.A. van Oijen and de Goey L.P.H., Modelling of premixed counterflow flames using the flamelet-generated manifold method, Combust. Theory Model. 6 (2002), pp. 463–478.

[12] Y.S. Niu, L. Vervisch, and P.D. Tao, An optimization-based approach to detailed chemistry tabulation: Automated progress variable definition, Combust. Flame 160 (2013), pp. 776–785.

[13] J. Chen, M. Liu, and Y. Chen, Optimizing progress variable definition in flamelet-based dimension reduction in combustion, Appl. Math. Mech. 36 (2015), pp. 1481–1498.

[14] M. Ihme, L. Shunn, and J. Zhang, Regularization of reaction progress variable for application to flamelet-based combustion models, J. Comput. Phys. 231 (2012), pp. 7715–7721.

[15] R.L.G.M. Eggels, *Modelling of combustion processes and no formation with reduced reaction mechanisms*, Ph.D. diss., Department of Mechanical Engineering, 1996.

[16] C. Strassacker, V. Bykov, and U. Maas, Parametrization and projection strategies for manifold based reduced kinetic models, Proc. Combust. Inst. 37 (2019), pp. 763–770.

[17] J.A. van Oijen, F.A. Lammers, and de Goey L.P.H., Modeling of complex premixed burner systems by using flamelet-generated manifolds, Combust. Flame 127 (2001), pp. 2124–2134.

[18] J.A. van Oijen, *Chem1d: A one-dimensional flame code*, Tech. Rep., Eindhoven University of Technology, 2013.

[19] G.R.A. Groot, J.A. van Oijen, De Goey L.P.H., K. Seshadri, and N. Peters, The effects of strain and curvature on the mass burning rate of premixed laminar flames, Combust. Theory Model. 6 (2002), pp. 675–695.

[20] A. Donini, *Advanced turbulent combustion modeling for gas turbine application*, Ph.D. diss., TUE: Department of Mechanical Engineering, 2014.

[21] de Swart J.A.M., G.R.A. Groot, J.A. van Oijen, ten Thije Boonkkamp J.H.M., and de Goey L.P.H., Detailed analysis of the mass burning rate of stretched flames including preferential diffusion effects, Combust. Flame 145 (2006), pp. 245–258.

[22] R.L.G.M. Eggels and De Goey L.P.H., Mathematically reduced reaction mechanisms applied to adiabatic flat hydrogen/air flames, Combust. Flame 100 (1995), pp. 559–570.

[23] A. Donini, R.J.M. Bastiaans, J.A. van Oijen, and De Goey L.P.H., Differential diffusion effects inclusion with flamelet generated manifold for the modeling of stratified premixed cooled flames, Proc. Combust. Inst. 35 (2015), pp. 831–837.

[24] A. Kazakov and M. Frenklach Reduced Reaction Sets based on GRI-Mech 1.2 available at http://www.me.berkeley.edu/drm/

[25] G.P. Smith, D.M. Golden, M. Frenklach, N.W. Moriarty, B. Eiteneer, M. Goldenberg, C.T. Bowman, R.K. Hanson, S. Song, W.C. Gardiner Jr., V.V. Lissianski, and Z. Qin, *GRI-Mech 3.0 reaction mechanism*; available at http://www.me.berkeley.edu/gri_mech/.

[26] J.A. van Oijen, *Flamelet-generated manifolds: Development and application to premixed laminar flames*, Ph.D. diss., TUE: Department of Mechanical Engineering, 2002.